

Near-field infrared nanospectroscopy reveals guest confinement in metal-organic framework single crystals

Annika F. Möslein,^a Mario Gutiérrez,^a Boiko Cohen^b and Jin-Chong Tan^{a*}

^aMultifunctional Materials & Composites (MMC) Laboratory, Department of Engineering Science, University of Oxford, Parks Road, Oxford OX1 3PJ, United Kingdom.

^bDepartamento de Química Física, Facultad de Ciencias Ambientales y Bioquímica, and INAMOL, Universidad de Castilla-La Mancha, Avenida Carlos III, S.N., 45071 Toledo, Spain.

*jin-chong.tan@eng.ox.ac.uk

Abstract

Metal-organic frameworks (MOFs) can provide exceptional porosity for molecular guest encapsulation useful for emergent applications in sensing, gas storage, drug delivery and optoelectronics. Central to the realisation of such applications however is the successful incorporation of the guest material within the host framework. Here we demonstrate, for the first time, the feasibility of scattering-type scanning near-field optical microscopy (s-SNOM) and nano-Fourier transform infrared (nanoFTIR) spectroscopy, in concert with density functional theory (DFT) calculations to reveal the vibrational characteristics of the Guest@MOF systems. Probing individual MOF crystals, we pinpoint the local molecular vibrations and thus, shed new light on the host-guest interactions at the nanoscale. Our strategy not only confirms the successful encapsulation of luminescent guest molecules in the porous host framework in single crystals, but further provides a new methodology for nanoscale-resolved physical and chemical identification of wide-ranging framework materials and designer porous systems for advanced applications.

Keywords:

Metal-organic frameworks, infrared nanospectroscopy, host-guest interaction, optical near-field microscopy, single crystals, nanoconfinement

INTRODUCTION

Metal-organic frameworks (MOFs), characterised by their crystalline hybrid structure, are constructed from metal clusters and organic linkers *via* self-assembly at the molecular level. MOFs exhibit remarkably large internal surface areas, far exceeding those found in

conventional porous materials such as zeolites and carbon black.¹ Merging the hybrid nature of MOFs with the ability to precisely tailor the characteristics of the pore yields multifunctional properties, boosting their deployment in emerging technologies ranging from gas storage and catalysis to luminescence, dielectrics, drug delivery and sensors.²⁻⁶ Due to their potential in prospective optoelectronic and sensing technologies, the research interest in luminescent MOFs has intensified over the last decade towards accomplishing MOF-based devices for real-world applications.⁷⁻⁹ In this context, the encapsulation of “guest” functional molecules into the “host” MOF pores is a versatile strategy to engineer the Guest@MOF composite materials with tuneable physicochemical properties arising from host-guest interactions.^{10, 11}

There are, however, outstanding challenges to be addressed to achieve the full potential of Guest@MOF systems. Particularly, it is very plausible that during the *in situ* synthesis or *ex situ* infiltration process, the guest molecules are adsorbed onto the external surfaces of MOFs instead of truly being encapsulated inside the pores. Unambiguously proving the latter is not a trivial task. Herein, we confirm – on single crystals – the fundamental encapsulation of luminescent guest molecules (fluorophores) into the framework structures of the MOF host material. Our nanoscale multimodal approach combines fluorescence lifetime imaging microscopy (FLIM) with precise determination of the vibrational dynamics of individual crystals, employing the scattering-type scanning near-field optical microscopy (s-SNOM) integrated with nano-Fourier transform infrared (nanoFTIR) spectroscopy.¹² The combination of the latter local-scale techniques enables us to perform single-crystal imaging and nanoscale chemical characterisation by measuring topography and infrared-active vibrational modes simultaneously.

Circumventing the diffraction limit of light, the s-SNOM technique offers capabilities well beyond the spatial resolution of conventional infrared (IR) spectroscopy.¹² The s-SNOM setup employed in this work is based on an atomic force microscope (AFM), where a platinum-coated cantilever tip serves as a topographical and near-field optical probe simultaneously (Fig. 1a). Key to the wavelength-independent resolution is the optical field enhancement confined to the apex of the AFM tip.¹³ Upon illumination, the probe induces an evanescent near-field by acting as a nanoscale light confiner, enhancer and scatterer (Fig. 1b). That way, as the tip polarises the sample, the optical near-field interaction between the metallic tip and the sample modifies the elastically scattered light. Interferometric detection provides sensitivity to measure the sample’s permittivity at a resolution comparable to the dimension of the tip apex.¹³ When this signal is Fourier transformed, sample-specific FTIR spectra with a spatial resolution of down to 20 nm are obtained (hereafter we refer to these length scales as “local”).^{14, 15} Significantly, and unlike conventional (far-field) IR spectroscopy techniques,

Fourier transformation of the interferogram yields near-field amplitude and phase signals simultaneously, because the sample is located at one of the interferometric arms.¹⁶

For the nanoFTIR method, the tip is operating in tapping mode at its mechanical resonance frequency ($\Omega = 250$ kHz) under illumination from a tuneable broadband IR laser. Demodulating the detector signal at higher harmonics of the tip oscillation frequency ($n\Omega$) extracts the near-field interaction from background contributions.¹⁷ Once normalised to a reference signal, this leads to the complex-valued near-field contrast, whose real part describes the nanoFTIR reflection. The imaginary part, correspondingly, defines the local nanoFTIR absorption comparable with the far-field FTIR absorption spectrum (further details in SI sections 1-2). s-SNOM imaging is achieved by using a monochromatic irradiation source instead of a broadband laser. In this case, the illumination wavelength is tuned close to an absorption band of interest to map the material surface on a 2D areal scan. Analogous to nanoFTIR, the scattered light is detected and deconvoluted at higher harmonics of the tip frequency to record the local optical properties through near-field contributions. Optical amplitude and phase now indicate regions of the sample's reflection and absorption at the specific wavelength to derive contrast images with nanoscale resolution.

In this work, we first demonstrate the efficacy of the near-field optical techniques for the physical and chemical characterisation of MOF single crystals (*ca.* 100s nm – 1 μ m). As a proof of concept, we measure nanoFTIR absorption spectra from individual crystals of zeolitic imidazolate framework ZIF-8 [$\text{Zn}(\text{mIM})_2$; mIM = 2-methylimidazolate],¹⁸ which represents a prototypical imidazole-based MOF with sodalite cage topology. We compare the near-field spectra with far-field FTIR measurements of a bulk sample, and with the theoretical spectra of ZIF-8. Subsequently, we demonstrate how to confirm the nanoscale confinement of luminescent guest molecules, such as rhodamine B (RhB) or fluorescein, encapsulated in ZIF-8 and UiO-66, the latter is a prototype of a highly stable zirconium-based framework [$\text{Zr}_6\text{O}_4(\text{OH})_4(\text{BDC})_6$; BDC = benzene-1,4-dicarboxylate].¹⁹ Specifically, we study the RhB@ZIF-8, RhB@UiO-66, and fluorescein@UiO-66 composite systems, finally validating the Guest@MOF concept.

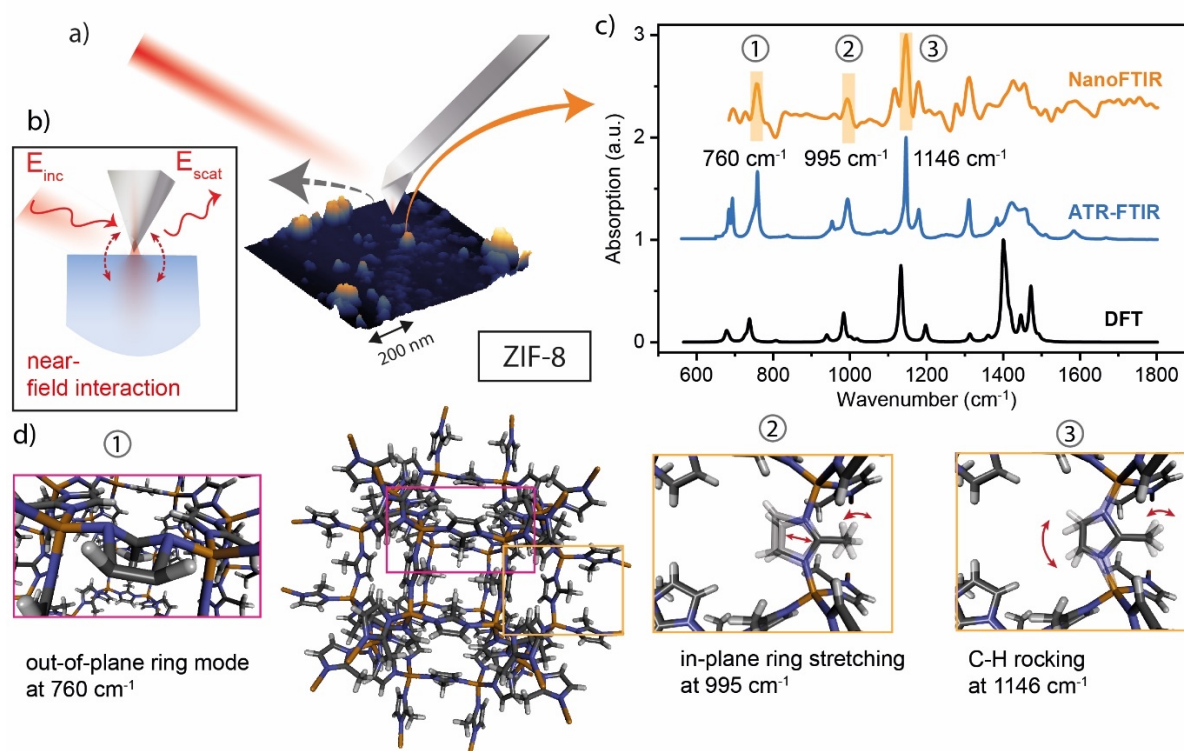


Figure 1: Near-field optical spectroscopy of individual ZIF-8 nanocrystals. (a) Representation of the setup of the s-SNOM measurement stage: the illuminated AFM tip generates a nanofocus on the sample. (b) The near-field interaction between the tip and the sample changes the scattered light from which the local optical properties of the sample are derived. (c) Mid-IR spectra of ZIF-8 crystals obtained *via* nanoFTIR and ATR-FTIR measurements, compared with the DFT calculations. The DFT spectrum was shifted by a factor of 0.97 to better match the experimental measurements.²⁰ (d) Characteristic vibrational modes of the ZIF-8 crystal structure: 1) out-of-plane deformation of the mIM ring at 760 cm^{-1} , 2) in-plane stretching of the mIM ring at 995 cm^{-1} and 3) C-H rocking of the mIM linker at 1146 cm^{-1} .

RESULTS AND DISCUSSIONS

IR spectroscopy of MOF single crystals

To begin with, we first investigate to what extent the described nanoFTIR method can be employed to probe individual MOF-type crystals. Herein, we compare the vibrational spectra of near-field nanoFTIR experimental measurements of ZIF-8 crystals with far-field attenuated total reflection (ATR-FTIR) measurements, and these experiments against *ab initio* quantum mechanical calculations from density functional theory (DFT). The results are shown in Fig. 1c. In the mid-IR region, the characteristic peaks at 760 cm^{-1} , 995 cm^{-1} and 1146 cm^{-1} are all fully resolved in the nanoscale measurements. Guided by DFT calculations of ZIF-8,²¹ we assign these vibrational bands to the out-of-plane and the in-plane ring stretching modes of the mIM linker, as well as the rocking mode of its C-H bonds, respectively, as illustrated in

Fig. 1d. Similarly, the in-plane ring bending modes of C-N bonds at 1116 cm^{-1} and 1311 cm^{-1} , as well as the symmetric C-N stretching mode at 1445 cm^{-1} are present in the nanoFTIR spectra.

Indeed, the matching IR spectra demonstrate the capability of nanoFTIR spectroscopy to characterise a MOF-type single crystal; nonetheless, this near-field technique yields minor changes in the IR spectrum. It is worth mentioning that our DFT calculation assumes a defect-free periodic crystal and neglects anharmonicity, while the far-field ATR-FTIR method measures the averaged response of a bulk (polycrystalline) powder material. In contrast, a local scale characterisation of individual single crystals can be achieved by leveraging nanoFTIR. As the latter is a surface technique with a probing depth of $\sim 20\text{ nm}$, surface effects might influence the IR spectrum. Close to the crystal boundary, where the framework symmetry is lost, some functional groups are surrounded by voids and air instead of their atomic neighbours assumed in a periodic crystalline structure. Such changes in the atomic environment will affect the strength of the bonds, altering their vibrational frequencies, and as a result, vibrational modes become more diverse. Hence, the nanoFTIR spectrum determined from the crystal surface exhibits additional peaks and relatively broader peaks (Fig. 1c). Although subtle alterations in the IR spectrum are observable, they can be explained by the nature of experimental surface measurements. In fact, nanoFTIR spectroscopy yields good agreement with established FTIR and DFT methods, furthermore it has the unique advantage to directly obtain a local IR spectrum reflecting the complex nature of a single MOF crystal whose size is of the order of $\sim 100\text{ nm}$.

Host-guest interactions at the nanoscale

In the case of MOFs, the nanoFTIR technique opens the door not only to the characterisation of the porous framework itself, but to gain a better understanding of the host-guest interactions in Guest@MOF systems by probing locally at the nanoscale. Crucially, one might ask whether the guest molecule is actually incorporated into the pore of the framework or adsorbed only to its external surfaces. To date, it has been a major challenge to unambiguously answer this question. Utilising nanoFTIR and s-SNOM imaging, for the first time, gives us the unique opportunity to chemically pinpoint the interaction of the guest molecule at the nanoscale with the MOF host.

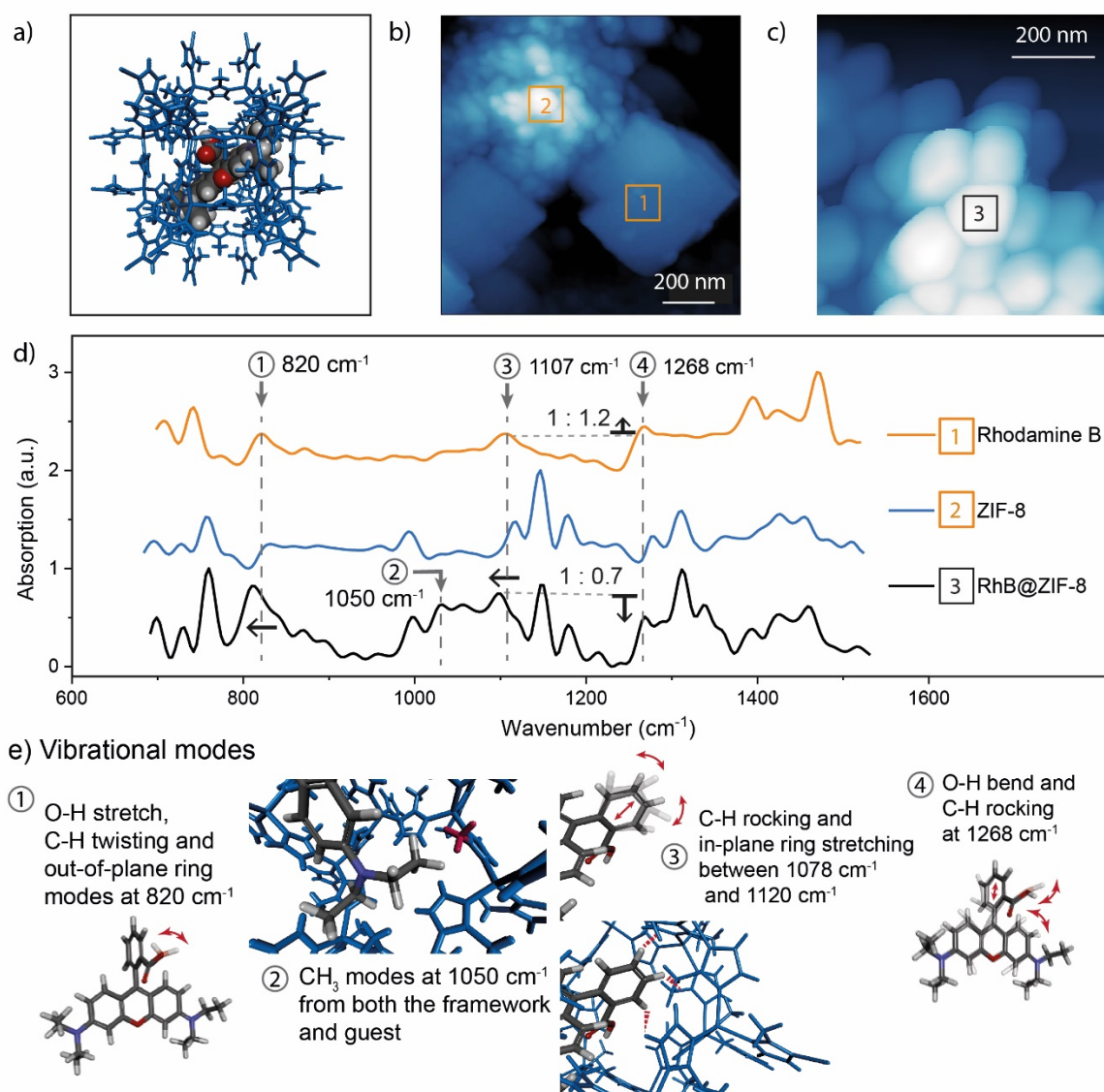


Figure 2: Vibrational analysis of rhodamine B (RhB) and ZIF-8 via nanoFTIR and DFT calculations. (a) Schematic representation of the RhB@ZIF-8 composite, depicting a RhB guest molecule being encapsulated in the pore of the ZIF-8 host framework (in blue). (b) AFM image of the as-synthesised sample containing two distinctive phases: (1) RhB and (2) ZIF-8 showing the positions where IR spectra were recorded. (c) AFM image of a single-phase sample of ZIF-8 nanocrystals adsorbing RhB. (d) nanoFTIR spectra determined at the designated locations on the AFM image. (e) Vibrational modes of the RhB@ZIF-8 composite illustrating the interactions between the ZIF-8 host framework and the RhB guest.

Here we consider an example Guest@MOF system, termed RhB@ZIF-8, comprising the luminescent rhodamine B (RhB) guest in ZIF-8 host, yielding a fluorescent material potentially useful for optoelectronics and photonic sensors.^{22, 23} However, the adsorption of RhB in pre-assembled ZIF-8 crystals only leads to surface interactions, since the size of the

RhB molecule (13.5 Å) exceeds the window aperture of the ZIF-8 pore (3.4 Å), thus hindering guest infiltration.²⁴ Therefore, we applied an *in situ* encapsulation of the RhB molecules during ZIF-8 formation to synthesise the RhB@ZIF-8 composite (see Methods and Fig. S3). Albeit, to isolate the RhB@ZIF-8 as synthesised, several washing steps were performed, AFM imaging still depicts different phases with round nanocrystals and micron-sized blocks as their distinct morphologies (Fig. 2b). Equally, local probing of the features with nanoFTIR spectroscopy at an illumination spot size of 20 nm yields two significantly different IR spectra. First, the cuboidal block is identified as pure RhB crystals through comparison with the DFT-simulated IR peaks (at 820 cm⁻¹, 1107 cm⁻¹, 1268 cm⁻¹, 1470 cm⁻¹ and 1576 cm⁻¹, calculated by Gaussian). Secondly, the frequencies measured at the individual round nanocrystals are matching the IR spectrum of pristine ZIF-8. Consequently, disparate regions of RhB and ZIF-8 are clearly distinguishable by nanoFTIR, where the topography and chemical fingerprint for each constituent material are identifiable without any indication of molecular interaction.

In the third region (Fig. 2c), the block crystals of RhB are absent, and the topography resembles the ZIF-8 nanocrystals. Interestingly, probing the individual crystals in this region yields an IR spectrum with characteristic features of both constituent materials (Fig. 2d). Although far-field FTIR measurements may equally lead to a combined IR spectrum, it is worth emphasising that this is due to the averaged probing over the bulk polycrystalline material without discriminating between the constituent materials present at the local scale. At the measured spot size of 20 nm, in contrast, the superposition of the aforementioned peaks reveals the concurrent presence of RhB and ZIF-8, leading to the conclusion that the RhB interacts with the ZIF-8 framework due to two reasons. First, all characteristic modes associated with the host framework were identified in the IR spectrum. Secondly, it can be seen that the vibrational bands assigned to RhB have been modified, revealing the interactions of the guest with the host framework. Considering the O-H group, for instance, with its stretch mode at 820 cm⁻¹ experiencing a small shift to lower energies, indicates an interaction between the O-H group of the guest molecule and the host framework, possibly with the Zn-atoms at defect sites.^{24, 25} Similarly, the bending mode of the O-H group at 1268 cm⁻¹ reveals a change in relative intensity with respect to the peak at 1107 cm⁻¹. We found that the CH₃ vibrations in the region around 1050 cm⁻¹, are reinforced due to superposition. The presence of both materials at a nanoscale spot demonstrates the interaction of RhB with the framework, however, this might be influenced by surface adsorption effects. We also observed reduced energy of the phenyl ring stretching modes in RhB at 1107 cm⁻¹ and 1118 cm⁻¹, which may indicate guest encapsulation. As the dimensions of the RhB molecule almost completely fill the pore of ZIF-8, upon confinement, the free-space vibrations of the trapped molecules are suppressed.

Confirming the confinement of RhB in the ZIF-8 framework

To further confirm the encapsulation of RhB guest molecules in the ZIF-8 host framework, we employ the s-SNOM imaging technique, as shown in Fig. 3. The illumination wavelength to identify ZIF-8 and RhB, respectively, was determined from a characteristic peak in the measured spectrum for each material (Fig. 3a). First, the applicability of the optical phase images, demodulated at the third harmonic of the tip frequency, is established. This is best done by considering regions with distinguishable material distribution, where both materials exhibit their distinct topographies (Fig. 3b). Upon illumination at 1146 cm^{-1} , only the ZIF-8 crystals absorb IR radiation, as shown by the red colour in the contrast image, whilst the RhB block appears as transparent as the gold substrate (blue colour). On the other hand, excitation at 1470 cm^{-1} leads to the inverted contrast due to the strong absorbance of the excited C=C modes of RhB. Hence, the selected illumination wavelengths are suitable to identify the distribution of RhB and ZIF-8 with nanoscale resolution, and further elucidate the presence of host-guest interactions.

As discussed earlier, one reason for the observed simultaneous presence of guest and framework material at a spot size of 20 nm may be attributed to surface adhesion. To eliminate any residual RhB from adhering on the surface of ZIF-8 nanocrystals, the synthesised RhB@ZIF-8 material was subjected to a second, more thorough washing process (see Methods in SI). If, despite any dye material being removed from the surface, the luminescent properties of RhB are still observable, then the luminescent guests shall be incorporated. On this basis, the material was thoroughly washed until the sample resembled the white colour of pristine ZIF-8 rather than the characteristic pink of RhB (Fig. 3c). Both the as-synthesised RhB@ZIF-8 (Fig. 3d) and the material obtained after thorough washing (Fig. 3e) were initially probed using s-SNOM imaging at the illumination wavelength of 1146 cm^{-1} to confirm the presence of ZIF-8 nanocrystals. When illuminated at 1470 cm^{-1} , a closer look reveals local inhomogeneity on the crystals isolated prior to exhaustive washing. Since the surface of the nanocrystals indicates regions where the distinctive wavelength for RhB is absorbed, we can unambiguously conclude that RhB is still attached to the surface. After thorough washing, however, no trace of RhB can be found on the surface of the ZIF-8 nanocrystals. The same phenomenon was observed at larger scan areas, where, for clarity, the optical phase contrast is normalised to demonstrate the excess RhB on the RhB@ZIF-8 material before washing. Note that a red contrast is also shown in the thoroughly washed material; this however can be assigned to a shadowing effect at the crystal edges (rather than originating from intrinsic

optical properties of the material), because only the areas surrounding the nanocrystals, unlike the crystals themselves, absorb light.

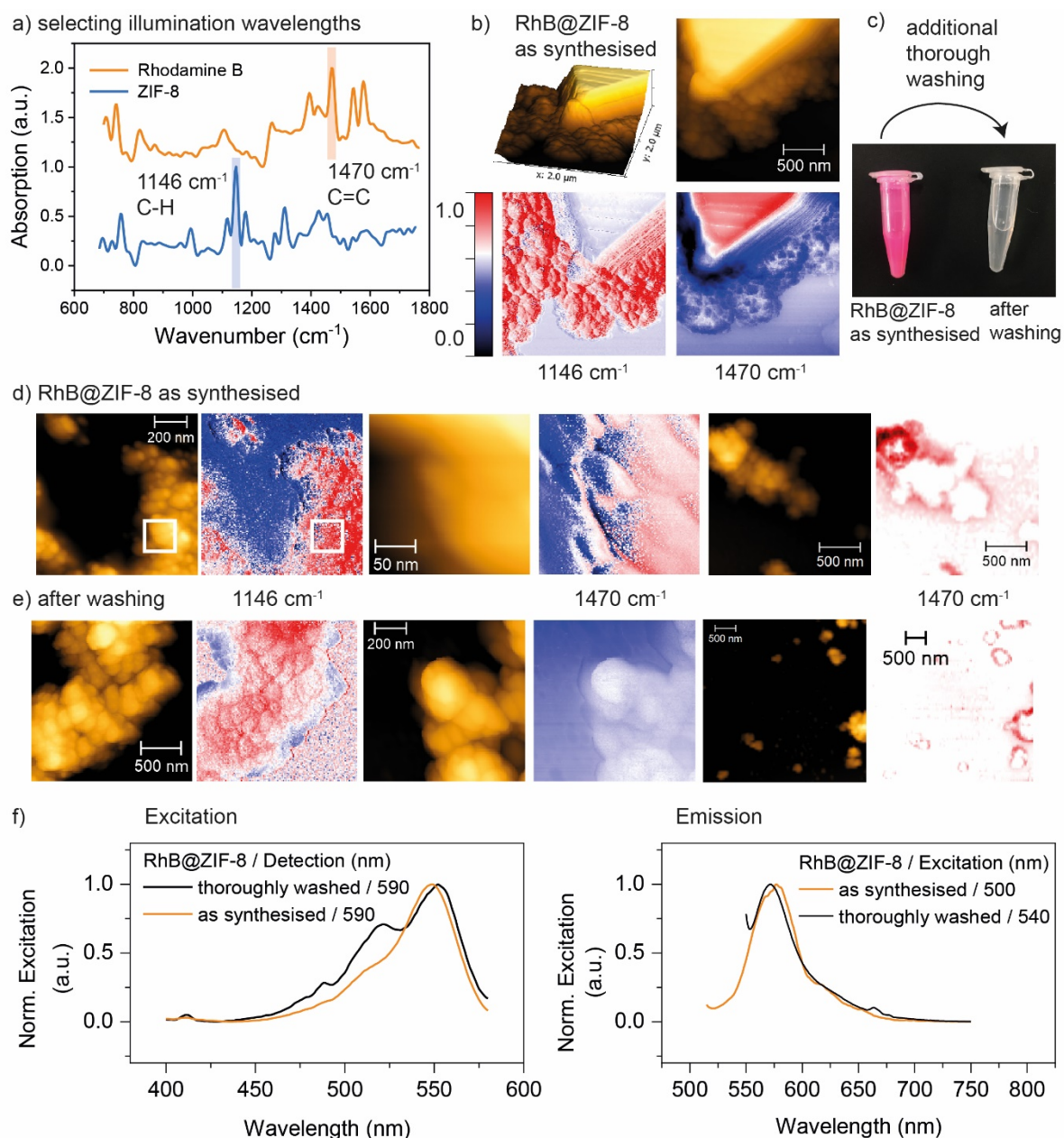


Figure 3: s-SNOM imaging of RhB@ZIF-8. (a) The illumination source was tuned to the characteristic peaks of RhB and ZIF-8. (b) Validation of the contrast images with known, distinguishable material distribution. (c) Samples before and after thorough washing, viewed under daylight. (d) AFM and near-field optical phase imaging of as-synthesised RhB@ZIF-8 with illumination at 1146 cm^{-1} confirming the presence of ZIF-8, and illumination at 1470 cm^{-1} still revealing RhB on the surface. (e) Near-field optical phase imaging of RhB@ZIF-8 after thorough washing, verifying the complete removal of residual RhB from the sample surface. (f) Normalised excitation and emission spectra of the as-synthesised and thoroughly washed RhB@ZIF-8 (dispersed in acetone) confirming the presence of RhB in both samples. Excitation and detection wavelengths are indicated in the figure.

s-SNOM imaging thus indicates the absence of RhB adhered onto the surface of the ZIF-8 nanocrystals (after thorough washing), with the removal of any excess guest material from the sample further confirmed by SEM imaging (Fig. S8). Remarkably, the excitation and emission spectra of the thoroughly washed RhB@ZIF-8 composite show the characteristic bands of RhB (Fig. 3f). Such observations from fluorescence spectroscopy reveal the presence of the luminescent dye within ZIF-8, which leads to the conclusion that the guest molecule is successfully encapsulated within the framework. Hence, this is a strong evidence verifying the formation of the RhB@ZIF-8 composite.

Revealing the guest encapsulation in UiO-66

To demonstrate the efficacy of the developed methodologies for determining the confinement of guest molecules in MOFs, we have employed two novel Guest@MOF systems as case studies: RhB@UiO-66 and fluorescein@UiO-66 (Fig. 4 and Fig. S4). We found that the as-synthesised RhB@UiO-66 still exhibits traces of excess guest material on the surface of the nanocrystals probed *via* nanoFTIR (Fig. 4a). Here, the peaks correlating to the characteristic modes of RhB (in the region between 820 cm^{-1} and 1268 cm^{-1}) are visible in the nanoFTIR spectrum in addition to the peaks of the pristine UiO-66 crystals (Fig. 4a). An exhaustive washing process eliminates any unconfined RhB and thus, the IR spectrum probed at nanoscale resolution on the surface of the crystals only reveals the representative peaks of UiO-66 (Fig. 4a). Turning to the fluorescein@UiO-66 system, likewise, after thoroughly removing any excess guest material, the nanocrystals were identified *via* nanoFTIR as UiO-66 without any sign of fluorescein on the surface (Fig. 4b).

AFM and SEM imaging of the thoroughly washed samples demonstrate the homogenous crystals without any excess guest material on the sample (Fig. 4c-d, Fig. S9). To further confirm the absence of the guest adhering on the surface, not only local point spectra but rather the surface of the fluorescein@UiO-66 crystals were examined using s-SNOM imaging for additional verification (Fig. 5b). Hereby, tuning the monochromatic irradiation source to the pronounced peak of UiO-66 at 1408 cm^{-1} illustrates the strong absorbance and reflectance of the crystals in comparison with the substrate. Little contrast, on the other hand, was obtained from illumination at 1325 cm^{-1} , a characteristic peak of fluorescein. Although some absorbance can be observed on the edges of the crystals, again, this can be attributed to noise and shadowing given that the same phenomenon emerges at a reference wavelength (1440 cm^{-1}), where neither fluorescein nor the UiO-66 material absorbs. Henceforth, the absence of any guest material adsorbed on the crystal surface is confirmed. As a proof for the confinement of the guest molecules within the framework, the emission and excitation spectra play a crucial

role. As opposed to the surface techniques, where no signal of the guest molecules is detected, the characteristic emission and excitation bands of RhB and fluorescein are clearly identified for RhB@UiO-66 and fluorescein@UiO-66 composites when measuring their photophysical properties (Fig. 5d-e).

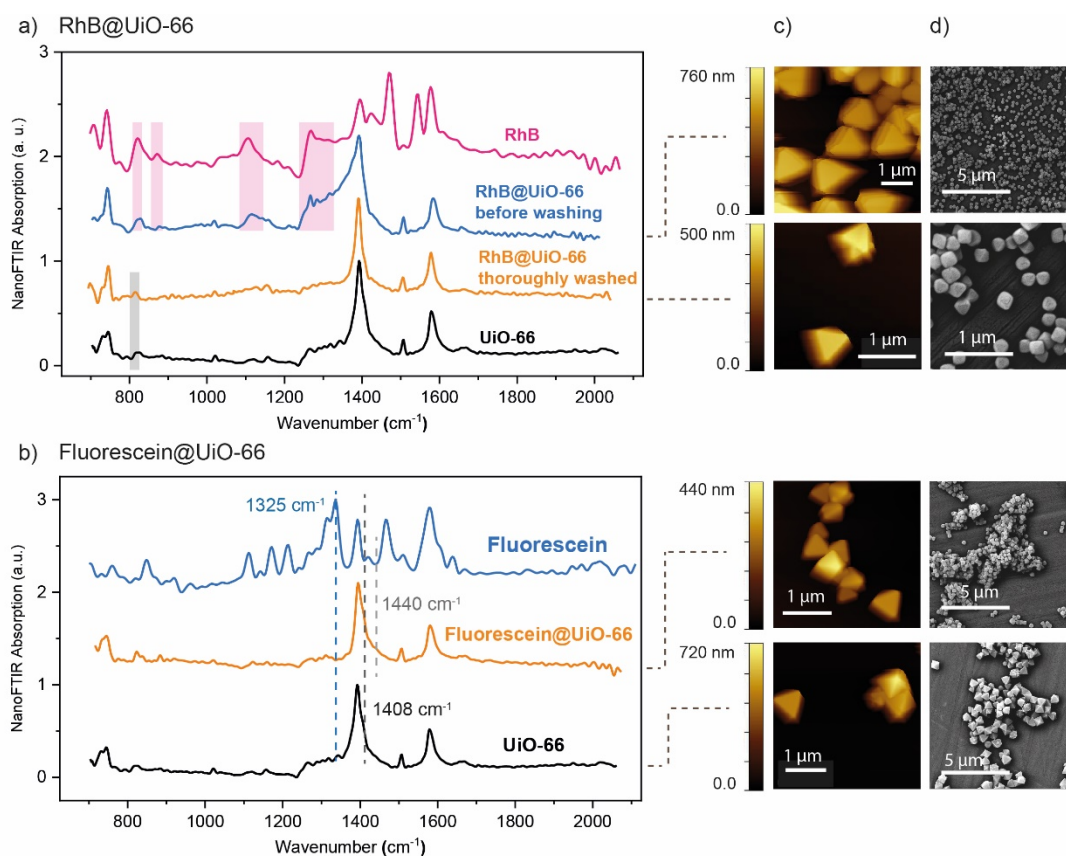


Figure 4: Near-field nanospectroscopy of UiO-66 single crystals with the encapsulated guest RhB and fluorescein, respectively. (a) Near-field IR absorption spectra of RhB, UiO-66, and as-synthesised RhB@UiO-66 composite (without washing the sample) and after thorough washing. (b) The nanoFTIR spectrum of fluorescein@UiO-66 measured on thoroughly washed nanocrystals revealing the absence of fluorescein on the sample surface. Distinguishable wavelengths are selected for subsequent s-SNOM imaging. (c) AFM and (d) SEM images of UiO-66, RhB@UiO-66 and fluorescein@UiO-66 crystals.

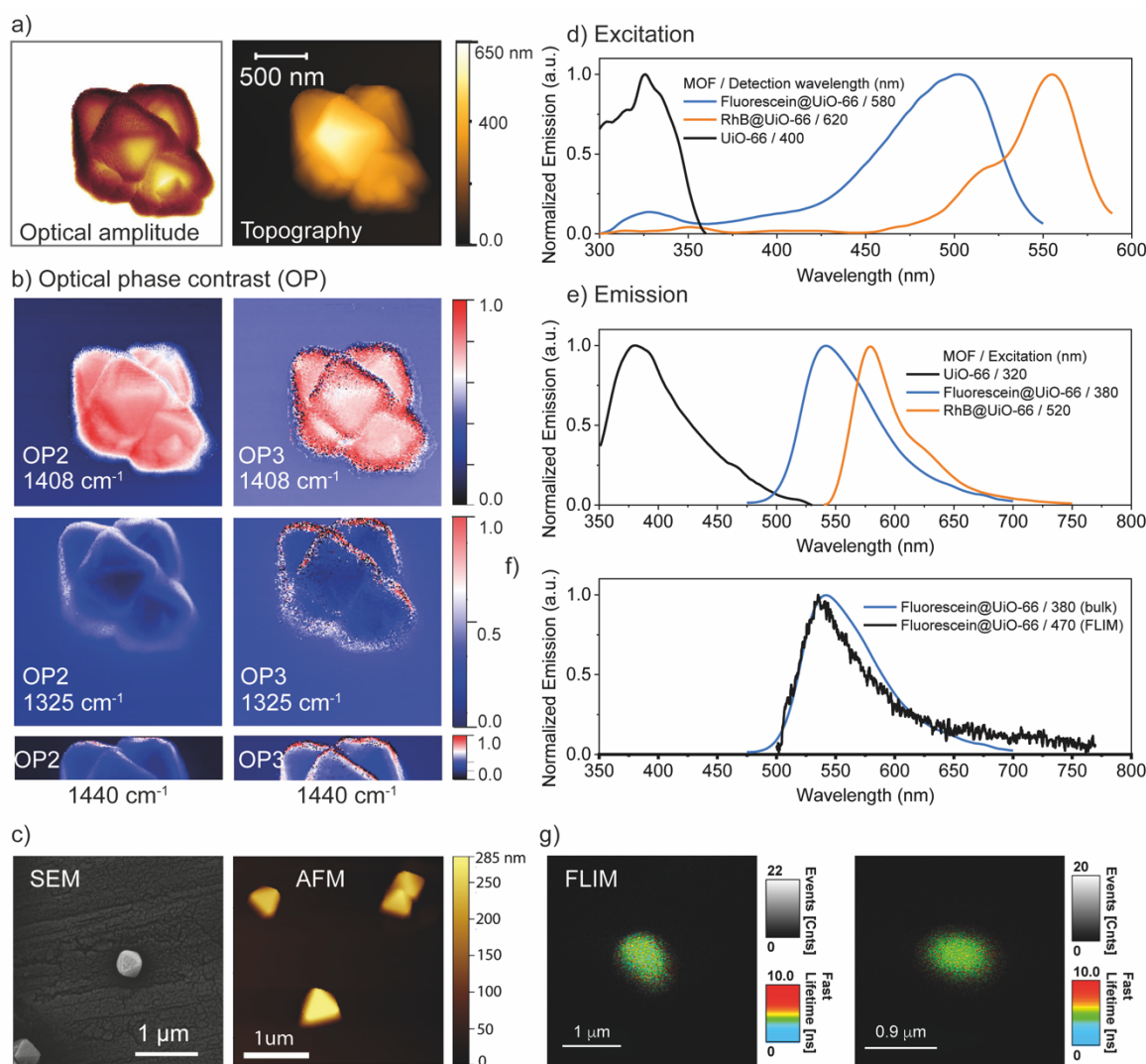


Figure 5: Nanoscale imaging confirming guest encapsulation in UiO-66. (a) Topography and optical amplitude imaging demonstrating the typical size and morphology of the crystals. (b) s-SNOM imaging proves that there are no traces of fluorescein on the surface of the UiO-66 crystals. The optical phase images were obtained *via* illumination at the major absorption peaks of UiO-66 (1408 cm^{-1}) and fluorescein (1325 cm^{-1}), and at a reference position (1440 cm^{-1}), as shown in figure 4b. (c) SEM and AFM imaging of the individual UiO-66 crystals. (d-e) Excitation and emission spectra of UiO-66 and thoroughly washed Guest@UiO-66 powder samples. Excitation and detection wavelengths are indicated in the figures. (f) Emission spectrum of a single crystal of fluorescein@UiO-66 obtained with a confocal fluorescence microscope compared with the spectrum of powder sample revealing the presence of fluorescein. (g) Fluorescence lifetime imaging microscopy (FLIM) confirming the encapsulation of fluorescein in UiO-66 single crystals, measured under an excitation wavelength of 470 nm.

Finally, to further corroborate the encapsulation of the fluorophores at a single crystal level, the fluorescence lifetime image (FLIM) of fluorescein@UiO-66 was recorded using a confocal

fluorescence microscope (see Methods in SI). Figure 5g shows two single-crystal FLIMs, where clearly, the fluorescein molecules are homogeneously distributed within the UiO-66 crystal. Moreover, the emission spectrum (Figure 5f) of these crystals correlates well with the emission of bulk fluorescein@UiO-66, proving that the emission signal is generated by the fluorescein guest molecules. The mean lifetime of the single crystals is a monoexponential decay of $\tau = 3.77 \pm 0.15$ ns (Figure S10) consistent with the lifetime of fluorescein in different solvents.²⁶⁻²⁸ This result suggests that fluorescein molecules are isolated in the form of monomers when partitioned by the pores, as the formation of aggregates will give multiexponential lifetimes.²⁹ The homogenous distribution of fluorescein molecules in the form of isolated monomers, alongside with the non-observation of fluorescein on the surface of UiO-66 crystals derived from the nanoFTIR experiments, unequivocally proves the encapsulation of the fluorophores into the MOF pores.

CONCLUSIONS

In summary, this first study of individual ZIF-8 and UiO-66 nanocrystals using near-field optical nanospectroscopy yields new understanding about MOFs and their host-guest interactions. We show the capability of the nanoFTIR methodology to characterise individual MOF-type crystals by comparison with established far-field techniques and *ab initio* theoretical calculations. Taking a step further towards precisely unravelling the physical and chemical properties of MOFs, we present the first near-field spectroscopic evidence of host-guest interactions by locally characterising both constituent materials at a 20 nm spot. A detailed analysis of the nanocrystals leveraging s-SNOM imaging confirms the absence of any guest material adsorbed on the surface (after thorough washing), while the photophysical properties of the luminescent molecules are still observable. We conclude that the guest molecule is confined in the framework and thus, evidencing the Guest@MOF concept. Our findings provide the groundwork to gain a fundamental understanding of the host-guest interactions underpinning hybrid framework materials, paving the way to controlling properties at the nanoscale — the key to engineer a multifunctional platform for nanotechnological applications.

ACKNOWLEDGEMENTS

A.F.M. thanks the Oxford Ashton Memorial scholarship for a DPhil studentship award. J.C.T. and A.F.M. thank the EPSRC Grant No. EP/N014960/1 and ERC Consolidator Grant under the grant agreement 771575 (PROMOFS) for funding. We would like to acknowledge the use of the University of Oxford Advanced Research Computing (ARC) facility in carrying out this

work (<http://dx.doi.org/10.5281/zenodo.22558>). We are grateful to the Research Complex at Harwell (RCaH) for the provision of advanced materials characterisation facilities. A.F.M. would like to thank Dr Cyril Besnard and Prof. Alexander Korsunsky for their help with SEM imaging, and neaspec GmbH for the opportunity to perform s-SNOM imaging in Haar, Germany. We also thank Dr Abhijeet Chaudhari for the provision of the RhB@ZIF-8 samples.

References

1. Furukawa, H.; Cordova, K. E.; O'Keeffe, M.; Yaghi, O. M. *Science* **2013**, 341 (6149), 1230444.
2. Zhu, L.; Liu, X. Q.; Jiang, H. L.; Sun, L. B. *Chem. Rev.* **2017**, 117 (12), 8129-8176.
3. Horcajada, P.; Gref, R.; Baati, T.; Allan, P. K.; Maurin, G.; Couvreur, P.; Ferey, G.; Morris, R. E.; Serre, C. *Chem. Rev.* **2012**, 112 (2), 1232-1268.
4. Li, B.; Wen, H. M.; Zhou, W.; Chen, B. *J. Phys. Chem. Lett.* **2014**, 5 (20), 3468-3479.
5. Lustig, W. P.; Mukherjee, S.; Rudd, N. D.; Desai, A. V.; Li, J.; Ghosh, S. K. *Chem. Soc. Rev.* **2017**, 46 (11), 3242-3285.
6. Ryder, M. R.; Zeng, Z.; Titov, K.; Sun, Y.; Mahdi, E. M.; Flyagina, I.; Bennett, T. D.; Civalleri, B.; Kelley, C. S.; Frogley, M. D.; Cinque, G.; Tan, J.-C. *J. Phys. Chem. Lett.* **2018**, 9 (10), 2678-2684.
7. Kaur, H.; Sundriyal, S.; Pachauri, V.; Ingebrandt, S.; Kim, K.-H.; Sharma, A. L.; Deep, A. *Coord. Chem. Rev.* **2019**, 401, 213077.
8. Stassen, I.; Burtch, N.; Talin, A.; Falcaro, P.; Allendorf, M.; Ameloot, R. *Chem. Soc. Rev.* **2017**, 46 (11), 3185-3241.
9. Gutiérrez, M.; Martín, C.; Van der Auweraer, M.; Hofkens, J.; Tan, J. C. *Adv. Opt. Mater.* **2020**, 2000670.
10. Allendorf, M. D.; Foster, M. E.; Leonard, F.; Stavila, V.; Feng, P. L.; Doty, F. P.; Leong, K.; Ma, E. Y.; Johnston, S. R.; Talin, A. A. *J. Phys. Chem. Lett.* **2015**, 6 (7), 1182-1195.
11. Chaudhari, A. K.; Kim, H. J.; Han, I.; Tan, J. C. *Adv. Mater.* **2017**, 29 (27), 1701463.
12. Knoll, B.; Keilmann, F. *Nature* **1999**, 399, 134-137.
13. Keilmann, F.; Hillenbrand, R. *Phil. Trans. R. Soc. A* **2004**, 362 (1817), 787-805.
14. Zenhausern, F.; Martin, Y.; Wickramasinghe, H. K. *Science* **1995**, 269, 1083-1085.
15. Huth, F.; Govyadinov, A.; Amarie, S.; Nuansing, W.; Keilmann, F.; Hillenbrand, R. *Nano Lett.* **2012**, 12 (8), 3973-3978.
16. Ocelic, N.; Hillenbrand, R. Optical device for measuring modulated signal light. US 7738115 B2, 2010.
17. Govyadinov, A. A.; Amenabar, I.; Huth, F.; Carney, P. S.; Hillenbrand, R. *J. Phys. Chem. Lett.* **2013**, 4 (9), 1526-1531.
18. Tan, J.-C.; Civalleri, B.; Lin, C.-C.; Valenzano, L.; Galvelis, R.; Chen, P.-F.; Bennett, T. D.; Mellot-Draznieks, C.; Zicovich-Wilson, C. M.; Cheetham, A. K. *Phys. Rev. Lett.* **2012**, 108 (9), 095502.
19. Cavka, J. H.; Jakobsen, S.; Olsbye, U.; Guillou, N.; Lamberti, C.; Bordiga, S.; Lillerud, K. P. *J. Am. Chem. Soc.* **2008**, 130 (42), 13850-13851.
20. Rauhut, G.; Pulay, P. *J. Phys. Chem.* **1995**, 99 (10), 3093-3100.
21. Ryder, M. R.; Civalleri, B.; Bennett, T. D.; Henke, S.; Rudic, S.; Cinque, G.; Fernandez-Alonso, F.; Tan, J. C. *Phys. Rev. Lett.* **2014**, 113 (21), 215502.
22. Zhang, Y. Q.; Wu, X. H.; Mao, S.; Tao, W. Q.; Li, Z. *Talanta* **2019**, 204, 344-352.
23. Chaudhari, A. K.; Tan, J. C. *Adv. Opt. Mater.* **2020**, 8 (8), 1901912.
24. Chin, M.; Cisneros, C.; Araiza, S. M.; Vargas, K. M.; Ishihara, K. M.; Tian, F. *RSC Adv.* **2018**, 8 (47), 26987-26997.
25. Zhang, C.; Han, C.; Sholl, D. S.; Schmidt, J. R. *J. Phys. Chem. Lett.* **2016**, 7 (3), 459.
26. Zhang, X. F.; Zhang, J.; Liu, L. *J. Fluoresc.* **2014**, 24 (3), 819-26.
27. Magde, D.; Rojas, G. E.; Seybold, P. G. *Photochem. Photobiol.* **1999**, 70 (5), 737-744.
28. Martin, M. M.; Lindqvist, L. *J. Lumin.* **1975**, 10 (6), 381-390.
29. Hungerford, G.; Benesch, J.; Mano, J. F.; Reis, R. L. *Photochem. Photobiol. Sci.* **2007**, 6 (2), 152-158.